arXiv:1906.03879v3 [astro-ph.SR] 12 Jun 2019

The period–luminosity relation of red supergiants with Gaia DR2

Filip W. Chatys,[1,2]★ Timothy R. Bedding,[1,2] Simon J. Murphy,[1,2] László L. Kiss[1,3,6] Dougal Dobie[1,4] and Jonathan E. Grindlay[5]

[1]*Sydney Institute for Astronomy, School of Physics, University of Sydney, NSW 2006, Australia*
[2]*Stellar Astrophysics Centre, Department of Physics and Astronomy, Aarhus University, DK-8000 Aarhus C, Denmark*
[3]*Konkoly Observatory, Research Centre for Astronomy and Earth Sciences, Hungarian Academy of Sciences, H-1121 Budapest,*
Konkoly Thege M. ut 15-17, Hungary
[4]*CSIRO Astronomy and Space Science, P.O. Box 76, Epping, New South Wales 1710, Australia*
[5]*Harvard University, Center for Astrophysics, Cambridge, MA USA*
[6]*MTA CSFK Lendület Near-field Cosmology Research Group*

ABSTRACT

We revisit the K-band period–luminosity (P–L) relations of Galactic red supergiants using Gaia Data Release 2 parallaxes and up to 70 yr of photometry from AAVSO and ASAS campaigns. In addition, we examine 206 LMC red supergiants using 50 yr of photometric data from the Digitised Harvard Astronomical Plate Collection. We identified periods by computing power spectra and calculated the period–luminosity relations of our samples and compared them with the literature. Newly available data tighten the P–L relations substantially. Identified periods form two groups: one with periods of 300–1000 days, corresponding to pulsations, and another with Long Secondary Periods between 1000 and 8000 days. Among the 48 Galactic objects we find shorter periods in 25 stars and long secondary periods in 23 stars. In the LMC sample we identify 85 and 94 red supergiants with shorter and long secondary periods, respectively. The P–L relation of the Galactic red supergiants is in agreement with the red supergiants in both, the Large Magellanic Cloud and the Andromeda Galaxy. We find no clear continuity between the known red giant period-luminosity sequences, and the red supergiant sequences investigated here.

Key words: stars: evolution – stars: late – type stars: supergiants –stars: pulsations – solar neighbourhood

1 INTRODUCTION

Red supergiants (RSGs) make up some of the brightest stars in the sky, with Betelgeuse (α Ori) and Antares (α Sco) being prominent examples. RSGs are bright enough that their variability can be studied in the Andromeda galaxy (M31) (see Soraisam et al. 2018). Pulsation in RSGs is common, and they are known to follow P–L relations, which we revisit with parallaxes from Gaia Data Release 2 (DR2; Gaia Collaboration et al. 2016, 2018).

RSGs are evolved, yet relatively young (≤ 20 M yr) stars. They burn helium in their cores and are very bright, i.e., 10^5–10^6 $L/L\odot$ (Humphreys & Davidson 1979) and moderately cool, with effective temperatures ranging from 3000 to 5000 K. Most of the flux of RSGs is emitted at red and infrared wavelengths, where W Cep and μ Cep, some of the brightest Galactic RSGs, have absolute K magnitudes brighter than -12 mag (see Section 4 for further discussion).

The lightcurves of RSGs are either semi–periodic or irregular, which led to a suggestion that their pulsations may be stochastically excited, with a strong contribution from the convective motions (Schwarzschild 1975, Christensen-Dalsgaard et al. 2001, Bedding 2003, Kiss et al. 2006). Changes in the circumstellar dust distribution and its composition from mass loss should also produce photometric variations in RSGs (Meynet et al. 2015). The dominant variability, however, is usually attributed to radial pulsations and follows a period–luminosity (P–L) relation (Kiss et al. 2006, Jurcevic et al. 2000, Yang & Jiang 2011 and Guo & Li 2002). RSGs are therefore potential "standard candles" for extragalactic distances (Glass 1979; Feast et al. 1980; Wood & Bessell 1985; Mould 1987).

★ E-mail: fcha8613@uni.sydney.edu.au

Another interesting property of RSGs, which they share with red giants (RGs), is the presence of long secondary periods (LSPs). These LSPs are observed in at least one third of RGs (Wood 2000, Soszyński et al. 2007), and their origins have been debated for decades. Binarity (Soszyński & Udalski 2014) and turnover of their giant convective cells (Stothers 2010) are the explanations most commonly suggested for the LSPs in RSGs, but no single mechanism has been accepted.

With the release of Gaia DR2 parallaxes (Gaia Collaboration 2018), our aim in this work is to update our knowledge about both the Galactic and the LMC RSGs. In Sections 2 and 3 we describe the selection of our samples, input catalogues and the data processing. Results are shown in Section 4, where we also revisit the P–L relation of the red giants.
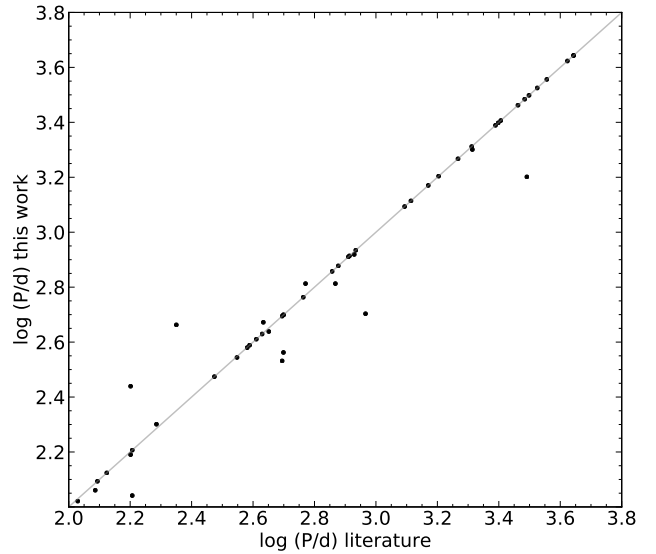
2   GALACTIC RED SUPERGIANTS

We chose a sample of 48 Galactic pulsating RSGs from Kiss et al. (2006), who measured periods using long-term visual observations from the American Association of Variable Stars Observers (AAVSO) database [1]. Gaia DR2 (Gaia Collaboration 2018) has delivered parallaxes with uncertainties smaller than 25% for 37 stars in this sample, up from 13 stars prior to DR2.

Our analysis of the long collections of the AAVSO photometry was supplemented by the 17-yr All Sky Automated Survey (ASAS) campaigns (ASAS-3 and ASAS-3N) (Pojmański 2004, Jayasinghe et al. 2018). Photometric measurements from ASAS used four different aperture diameters: 3, 4, 5 and 6 pixels (MAG0, MAG1, MAG2, MAG3 and MAG4, respectively, as per the ASAS nomenclature). We used the widest aperture MAG4 to capture all the flux, since contamination was not an issue for such bright objects. We analysed all available ASAS datasets (up to four available per star), each representing a different ASAS field. We found offsets in photometric measurements between both the consecutive ASAS campaigns, as well as fields within the same campaign, and in some overlapping areas magnitudes differed by as much as 0.1 mag. The offsets in lightcurves between AAVSO (visual estimates) and each ASAS campaign (photometry with CCD detectors) were corrected by giving the ASAS time series the same median as the AAVSO data.

2.1   Period analysis

From AAVSO data, we included observations of the observers who observed for more than 30 days in total. We then binned the lightcurves into 10, 30 and 50-d bins to: (i) minimise the effect of outliers; (ii) balance out a difference in the relative weight of the measurements between ASAS (10-yr data) and the AAVSO (at least couple of decades); (iii) make detection easier of both, shorter and longer periods (10, 30-d bins for shorter periods and 50-d bins for longer periods). The ASAS time-series were binned into 10-d

Figure 1. Comparison of periods of Galactic RSGs, from this study (y-axis) with the literature (Kiss et al. 2006, Percy & Khatu 2014) (x-axis). The grey line shows equality. Stars with periods, which do not agree with the literature are marked with asterisk in Table 1.

groups. We also de-trended the AAVSO lightcurves (by subtracting a linear fit from the lightcurve) to prevent a low frequency peak from dominating the Fourier spectrum.

We used the Lomb-Scargle periodogram (Lomb 1976; Scargle 1982) to calculate the power spectra and identify periods. We inspected the power spectra between frequencies of 0.01 0.0001 d^{-1} (100–10000 d), and searched for any distinguishable peaks. The software PERIOD04 (Lenz & Breger 2005) was used to subtract the peak signal from the lightcurve and perform a second Fourier analysis on the residuals. When detecting periodicities, we checked against the previously identified periods (Kiss et al. 2006, Wasatonic et al. 2015, Percy & Khatu 2014), both for consistency and to see whether there is any improvement in the findings with the recent years of data added. Figure 1 compares our measured periods with the literature (43 periods agreed to within 10%).

Representative lightcurves and power spectra are shown in Fig. 2 for the stars BC Cyg, VY CMa and VX Sgr. Notably, over half of our sample (27 objects) exhibit a periodicity in AAVSO data close to one year (although not the most dominant peak in the power spectrum). Kiss et al. (2006) suggested that this effect could be caused by a seasonal variation in visibility resulting in a differential extinction of a few tenths of a magnitude. Another possibility is the Ceraski effect, described by Percy & Khatu (2014), which affects visual observers only. When they observe two stars of equal brightness that are aligned perpendicularly to the line of sight (which happens at certain times of the year), they perceive the upper star to be brighter than the one below. We omitted annual peaks from further analysis except for five stars (AZ Cyg, α Ori, WY Gem, BU Per, α Her) that had these periods validated by the ASAS data.

We measured amplitudes from the height of the peak in the Fourier spectrum, which gives the semi–amplitude of the best–fitting sinusoid. Note that amplitudes in the literature

are often given as peak-to-peak values (e.g. in Yang & Jiang 2011), which would be twice the values we measured. We show the ASAS amplitudes in Table 1, which are based on CCD measurements in the V filter.

Table 1 shows the Galactic sample with stars ordered by their brightness (descending). Column 1 shows star name, next is HD catalogue number, identified periods, amplitudes and apparent K magnitude. Parallax and the associated uncertainty are in columns 10 and 11, respectively. Calculated absolute K magnitudes and uncertainties are shown in columns 12, 13 and 14. Sources of parallaxes and K-band magnitudes are described in Sections 2.2 and 2.3, respectively.

2.2 Parallaxes

Some targets have parallaxes from multiple sources, in which case we used the measurement with the smallest uncertainty. These are shown in Fig. 3. We took 37 parallaxes from Gaia DR2, seven from Hipparcos (van Leeuwen 2007) and one from Gaia DR1 (DR1; Gaia Collaboration 2016). Two objects, W Ind and W Cep, have large fractional uncertainties of 0.57 (from DR1) and 1.0 (from DR2), respectively, and these stars have not been shown in Fig. 3.

We calculated distances by inverting the parallaxes. Because this can be a biased distance estimator (Lutz & Kelker 1973, Bailer-Jones et al. 2018; Lindegren et al. 2018; Luri et al. 2018), we compared these with distances from the Bailer-Jones et al. (2018) catalogue. Note that the Bailer-Jones et al. (2018) included a global parallax zero-point of −0.029 mas (Lindegren et al. 2018). Once this was taken into account, we found excellent agreement, which confirms that for small values of fractional parallax (<0.2), the Bailer-Jones et al. (2018) posteriors are approximately Gaussian with a mode close to the inverse parallax (Bailer-Jones 2015; Bailer-Jones et al. 2018). Since other zero-point offset values have been suggested for the DR2 parallaxes (Lindegren et al. 2018; Riess et al. 2018; Zinn et al. 2018; Stassun & Torres 2018; Khan et al. 2019), we proceeded with the inverse parallax distances, without any correction. However, we consider the impact of the zero-point offset on the calculated absolute magnitudes of the Galactic RSGs and their P–L relation in Sec. 4.2.

The majority of the sample (75%) have fractional parallax uncertainties below 0.20 and the so-called renormalized unit weight error (RUWE) below 1.4 (threshold from Lindegren et al. 2018), which is what the Gaia team recommends when filtering on the unit weight error described in appendix C of Lindegren et al. 2018. However, we need to treat the DR2 uncertainties with caution because the associated astrometric measurements (excess noise, excess noise significance and goodness-of-fit) for these stars indicated low–quality fits. This may result from large–scale convective motions, which generate surface brightness and colour asymmetries, causing a shift of the photocentre that Gaia measures (Chiavassa et al. 2018). Saturation could be another reason for large uncertainties, since 33 Galactic RSGs have G < 7 mag, with 14 stars brighter than 6 mag.

Table 1 shows the DR2 parallaxes and uncertainties used in the analysis. We calculated (and showed in Table 1) the upper limit on the M_K of W Cep by assuming 0.1 mas as an upper limit on the parallax. Finally, there are three objects,

S Per (Asaki et al. 2010), VY CMa (Zhang et al. 2012) and PZ Cas (Kusuno et al. 2013), that have accurate trigonometric parallaxes determined from measurements of the H_2O (S Per, PZ Cas) and SiO (VY CMa) masers.
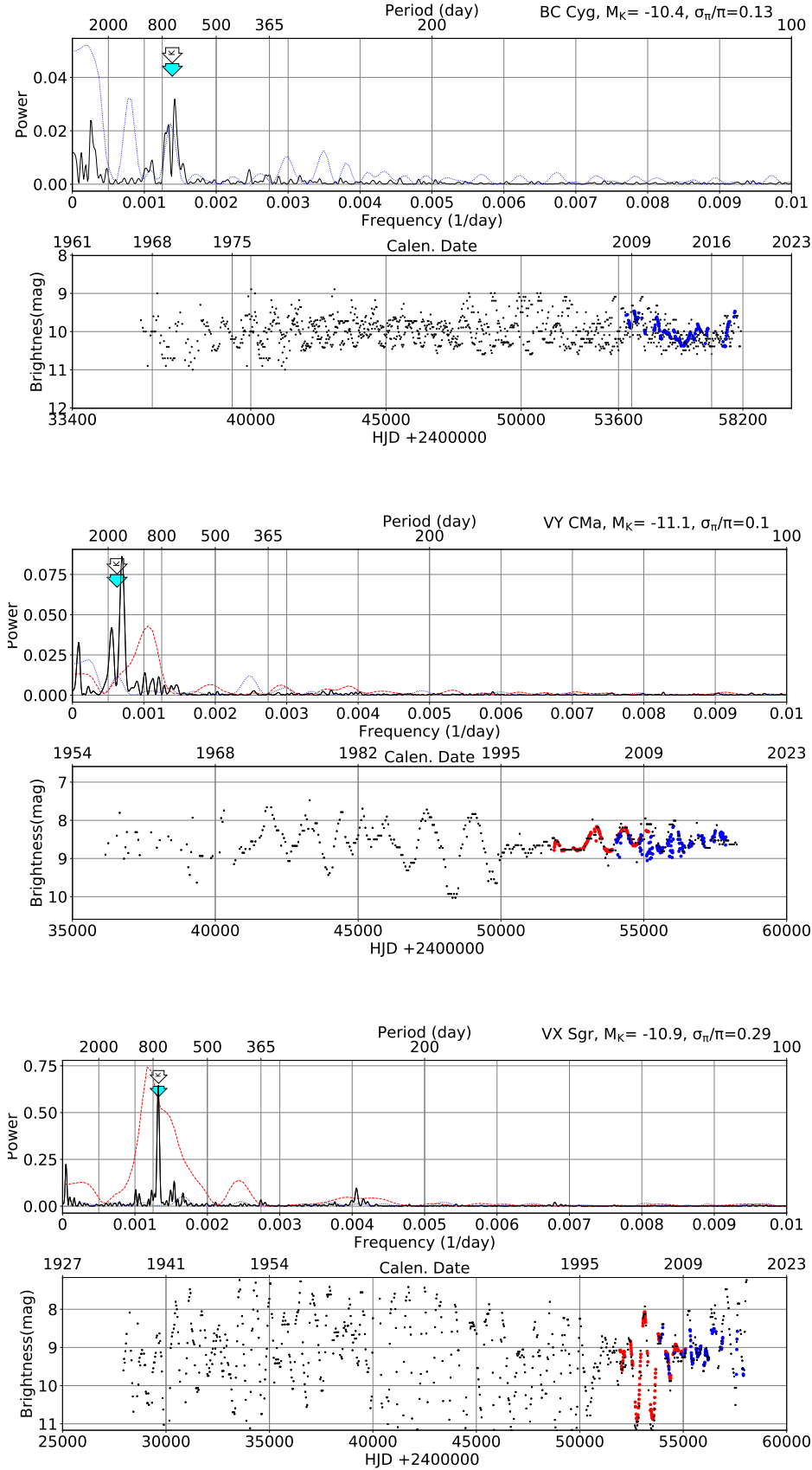
2.3 Apparent K-band magnitudes

Photometry of red supergiants can be significantly affected by interstellar and/or circumstellar dust (Josselin et al. 2000, Massey et al. 2005). V band data typically shows a larger spread in the observed magnitudes than the near–infrared (NIR) photometry, where the bolometric and extinction corrections are smaller (Cardelli et al. 1989), and where changes in the observed variability due to pulsation are smaller (Josselin et al. 2000; Kiss et al. 2006; Massey et al. 2009). In addition, fluxes of these objects peak in the NIR, and for these reasons, we followed previous studies of the P–L relation of RSGs in using K-band magnitudes.

To collect K-band apparent magnitudes, we followed the process described in Tabur et al. (2009) and searched the available NIR catalogues: Catalogue of Infrared Observations (CIO, Gezari et al. 1999) and Diffuse Infrared Background Experiment archive (DIRBE Catalogue of Stellar Photometry in Johnson's, Ducati 2002). We used the Gezari K-band magnitudes for 43 stars and the Two Micron All Sky Survey (2MASS) catalogue (Cutri et al. 2003) for three objects (CK Car, AO Cru and PP Per). EV Car and UZ CMa were sourced in Catalogue of Stellar Photometry in Johnson's 11-color system and DIRBE data, respectively. We combined the CIO observed magnitudes (at a wavelength of $2.2 \pm 0.05 \ \mu$m) to calculate a median K magnitude for each star, weighted equally because the catalogue did not provide uncertainties of the measurements. For the majority of our sample, K magnitude uncertainties were not published. We calculated absolute magnitudes using the relation $M = m + 5 + 5 \log \pi$, where m is the apparent magnitude, and π is the parallax in arcseconds. The values are presented in Table 1, with further discussion in Section 4.2.

3 RED SUPERGIANTS IN THE LMC

The Digital Access to Sky Century @ Harvard (DASCH; Grindlay et al. 2012; Tang et al. 2013) program is digitising the Harvard Astronomical Plate Collection, which consists of tens of thousands of photographic plates spanning most of the 20th century. These include the plates in the Small Magellanic Cloud that Henrietta Swan Leavitt used to determine the P–L relation in Cepheid variables (Leavitt & Pickering 1912). Our work uses the Large Magellanic Cloud plates, which have been recently digitised. Most stars we used have observation spanning approximately 10 000–20 000 days, or 30–55 yr.

We obtained our list of 206 supergiants primarily from Yang & Jiang (2011) (190 objects), with the other objects taken from Massey & Olsen (2003) (No.205, 208, 209, 210, 216 and 217), Boyer et al. (2011) (No.191, 195, 196, 199 and 200), Catchpole & Feast (1981) (No.227), Kastner et al. (2008) (No.219, 220 and 225) and Levesque et al.

Figure 2. Sample AAVSO (50-d bins) and ASAS (10-d bins) lightcurves with associated power spectra of three Galactic RSGs, BC Cyg, VY CMa and VX Sgr. Filled arrows indicate adopted pulsational periods and white arrows with K mark periodicity published by Kiss et al. (2006). Black, red and blue colours indicate AAVSO, ASAS-3 and ASAS-3N data respectively (All lightcurves are available in the supplementary material).

Table 1. Galactic sample of RSGs. Stars are ordered by their absolute *K* magnitudes. P1, P2 and P3 indicate the periods identified in this study with their associated amplitude values shown in amp1, amp2, amp3 columns. Parallax and the associated uncertainty are in the columns 10 and 11. The parallax sources are given in Section 2.2. Calculated absolute *K* magnitudes and uncertainties are shown in columns 12, 13 and 14. Asterisks mark objects for which determined periods do not agree with the literature to within 10%.

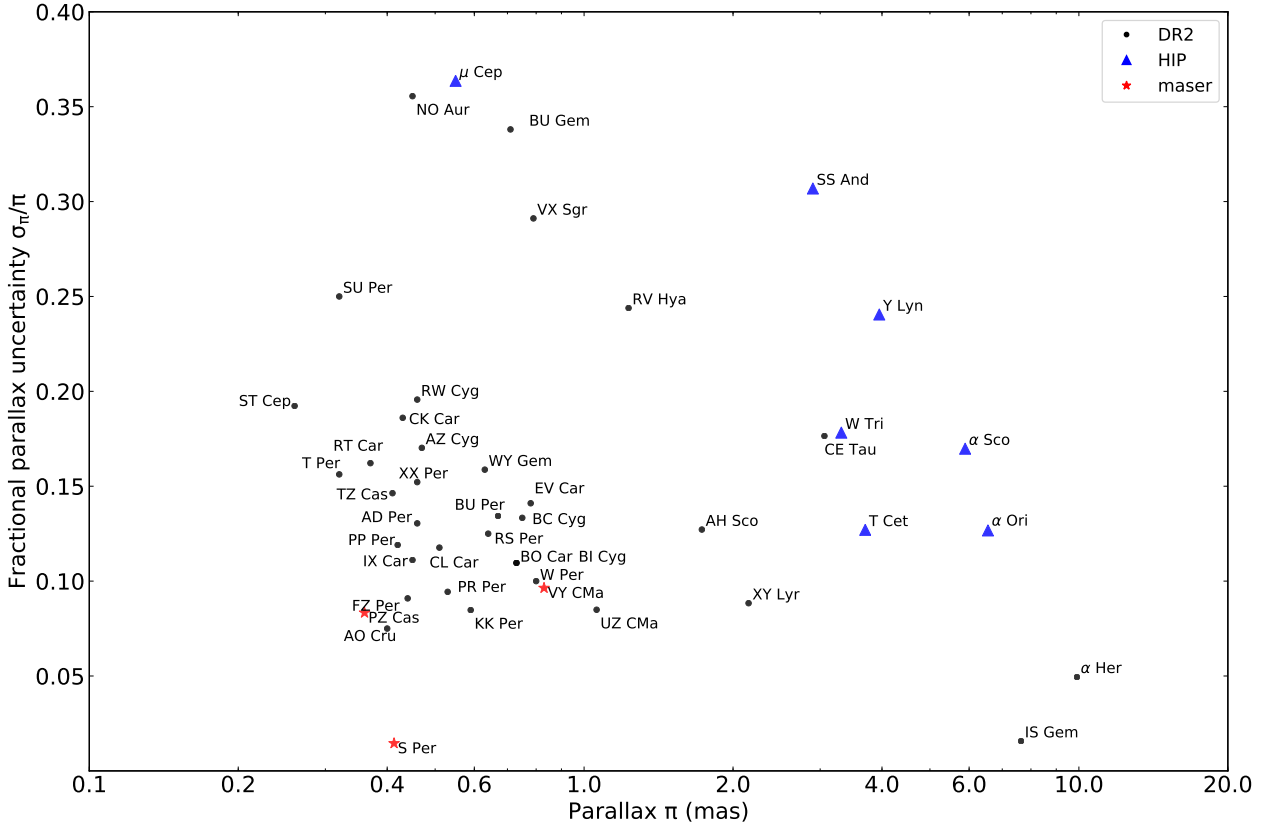| Name	HD	P1 (day)	amp1 (mag)	P2 (day)	amp2 (mag)	P3 (day)	amp3 (mag)	K	π (mas)	σ_π (mas)	M_K	σ_{M_K} (+)	σ_{M_K} (−)
W Cep	214369	10000	0.24	—	—	—	—	2.35	0.05	0.05	<−12.65	—	—
μ Cep	206936	860	0.06	4400	0.13	—	—	−1.67	0.55	0.20	−12.97	0.67	−0.98
TV Gem	42475	426	0.1	2550	0.17	—	—	0.91	0.32	0.13	−11.57	0.25	−0.28
PZ Cas	37536	830	0.21	—	—	—	—	0.98	0.36	0.03	−11.24	0.38	−0.46
RW Cyg	—	580	0.19	—	—	—	—	0.52	0.46	0.09	−11.17	0.39	−0.47
ST Cep	239978	610	0.15	—	—	—	—	1.80	0.26	0.05	−11.13	0.38	−0.46
VY CMa	58061	1600	0.2	—	—	—	—	−0.69	0.83	0.08	−11.09	0.20	−0.22
SU Per	14469	470	0.1	3050	0.24	—	—	1.45	0.32	0.08	−11.03	0.48	−0.62
VX Sgr	165674	754	0.85	—	—	—	—	−0.40	0.79	0.23	−10.91	0.55	−0.75
NO Aur	246070	—	—	—	—	—	—	0.88	0.45	0.16	−10.85	0.66	−0.95
S Per	14528	813	0.44	—	—	—	—	1.45	0.41	0.01	−10.47	0.03	−0.03
CK Car*	90382	505	0.14	—	—	—	—	1.36	0.43	0.08	−10.47	0.37	−0.45
AZ Cyg*	—	340	0.1	495	0.14	3350	0.23	1.22	0.47	0.08	−10.42	0.34	−0.41
BC Cyg	—	720	0.18	—	—	—	—	0.21	0.75	0.10	−10.41	0.27	−0.31
RT Car	—	435	0.22	2000	0.13	—	—	1.86	0.37	0.06	−10.30	0.33	−0.38
BI Cyg	—	4350	0.14	—	—	—	—	0.59	0.73	0.08	−10.09	0.23	−0.25
TZ Cas*	—	475	0.06	1590	0.13	—	—	1.89	0.41	0.06	−10.05	0.30	−0.34
α Sco	148478	—	—	—	—	—	—	−3.82	5.89	1.00	−9.96	0.34	−0.40
α Ori	39801	388	0.08	2050	0.07	—	—	−4.00	6.55	0.83	−9.92	0.26	−0.29
IX Car	94096	408	0.15	4400	0.15	—	—	1.86	0.45	0.05	−9.88	0.23	−0.26
XX Per	12401	3150	0.03	—	—	—	—	1.81	0.46	0.07	−9.88	0.31	−0.36
T Per	14142	2500	0.07	—	—	—	—	2.66	0.32	0.05	−9.81	0.32	−0.37
AO Cru	106873	3700	0.12	—	—	—	—	2.20	0.40	0.03	−9.79	0.16	−0.17
CL Car*	94599	500	0.35	1400	0.26	—	—	1.68	0.51	0.06	−9.78	0.24	−0.27
BU Gem	42543	2450	0.19	—	—	—	—	0.98	0.71	0.24	−9.77	0.63	−0.90
EV Car	89845	820	0.67	—	—	—	—	0.90	0.78	0.11	−9.64	0.29	−0.33
AD Per	14270	—	—	—	—	—	—	2.09	0.46	0.06	−9.60	0.27	−0.30
RS Per*	14488	460	0.14	4200	0.22	—	—	1.68	0.64	0.08	−9.29	0.26	−0.29
BO Car	93420	—	—	—	—	—	—	1.42	0.73	0.08	−9.26	0.23	−0.25
FZ Per	14330	—	—	—	—	—	—	2.55	0.44	0.04	−9.24	0.19	−0.21
WY Gem	42474	350	0.1	—	—	—	—	1.83	0.63	0.10	−9.17	0.32	−0.38
PR Per	14404	—	—	—	—	—	—	2.34	0.53	0.05	−9.04	0.20	−0.22
RV Hya	73766	195	0.13	950	0.17	—	—	0.52	1.23	0.30	−9.04	0.47	−0.61
KK Per	13136	170	0.06	300	0.08	1850	0.1	2.12	0.59	0.05	−9.03	0.18	−0.19
PP Per	—	—	—	—	—	—	—	2.95	0.42	0.05	−8.93	0.24	−0.28
W Ind	201866	200	0.5	—	—	—	—	1.21	1.02	0.58	−8.75	0.98	−1.83
XY Lyr	172380	115	0.1	—	—	—	—	−0.29	2.15	0.19	−8.62	0.18	−0.20
BU Per	—	380	0.14	3600	0.21	—	—	2.26	0.67	0.09	−8.61	0.27	−0.31
α Her*	156014	124	0.04	365	0.06	1480	0.05	−3.51	9.91	0.49	−8.53	0.10	−0.11
AH Sco*	155161	650	0.5	—	—	—	—	0.31	1.73	0.22	−8.50	0.26	−0.30
W Per	237008	500	0.22	2900	0.28	—	—	2.00	0.80	0.08	−8.48	0.21	−0.23
CE Tau	36389	1300	0.08	—	—	—	—	−0.89	3.06	0.54	−8.46	0.35	−0.42
T Cet*	1760	110	—	161	—	298	—	−0.81	3.70	0.47	−7.97	0.26	−0.29
UZ Cma*	—	160	2	—	—	—	—	2.35	1.06	0.09	−7.52	0.18	−0.19
Y Lyn	58521	133	0.1	1240	0.33	—	—	−0.46	3.95	0.95	−7.48	0.47	−0.60
SS And	218942	155	0.13	275	0.13	—	—	0.97	2.90	0.89	−6.72	0.58	−0.80
W Tri	16682	105	0.07	650	0.06	—	—	1.07	3.31	0.59	−6.33	0.36	−0.43
IS Gem	49380	—	—	—	—	—	—	2.71	7.64	0.12	−2.87	0.03	−0.03

(2006) (No.223). We queried the DASCH online database [2] with a search radius of 5 arcsec and determined the correct star by looking at the magnitude and position. We extracted time and brightness data (uncertainties were not used in this study) and processed them using the same method as the Galactic sample (see Sec. 2.1), except a bin size of 10 d was used, since the available time span of the DASCH observa-

tions was shorter than the AAVSO data. We trimmed each lightcurve so it only contained measurements on the interval 2 420 000–2 440 000 (JD), where the majority of useful observations occurred.

We completed Fourier analysis using the same methodology and software that were used for the Galactic RSGs. We searched for frequencies between 0.000125 and 0.01 d^{-1}, corresponding to periods of 100–8000 d.

Out of the 206 objects we selected 170 lightcurves for further analysis; the other 36 were either not available in

Figure 3. Fractional parallax uncertainty measurements taken by Gaia DR2, Hipparcos and masers (see Section 2.2 for details). W Ind and W Cep with $\sigma_\pi/\pi = 0.57$ and 1.0, respectively, have not been shown. BO Car and BI Cyg, with the same parallax and uncertainties values ($\pi = 0.73$ mas and 0.08 mas), are indicated by one mark.

DASCH or had poor-quality or sparse lightcurves. We inspected the power spectra and lightcurves of these 170 objects and found periods in 142 (83%). The rest had power spectra dominated by $1/f$ noise with no clear periodicity. In Fig. 4 we show three examples (stars No.003, 043, 083) of the lightcurves and power spectra with identified periods.

In Figure 5 we compare the DASCH shorter periods of 32 LMC RSGs, with values from Yang & Jiang (2011). For the majority of objects (81%), these agree to within 15%. Disagreement can result from the stochastic nature of periodicity if observations are taken at different times. Because DASCH data have longer timespans, we used our periods in preference to the literature values. We note that we do not show LSPs, published by Yang & Jiang (2011) because they were based on only 3000 d of data (mostly ASAS), which we consider too short for a reliable detection of LSPs.

Table 2 shows the LMC sample with stars numbered as per Yang & Jiang (2011). Columns 2 and 3 present coordinates of the stars, followed by identified periods, the associated amplitudes, K magnitudes, their uncertainties and the absolute K magnitudes. We list all 206 objects that form our LMC sample. Stars without periods can be classified into four groups – (i) those without enough data to perform a reasonable Fourier transform, (ii) those with high noise in the Fourier transform (making it unreasonable to determine a period), (iii) those with unreliable periods $\gtrsim 8\,000$ d, and

(iv) six objects for which the DASCH database did not provide a time series.

We took K-band magnitudes of the LMC stars from the 2MASS catalogue (Cutri et al. 2003). Most stars have a magnitude uncertainty of less than 0.03 mag, which is shown in Table 2. We adopted a distance modulus of $\mu(\text{LMC}) = 18.476$ mag (Pietrzyński et al. 2019).

4   RESULTS AND DISCUSSION

4.1   Period–Luminosity Relation

Figure 6 shows P–L diagram (M_K versus log P) for our samples, with Galactic RSGs shown with two different thresholds on the parallax uncertainties (15% and 25%). In addition to the RSGs analysed in this study, we show RSGs in M31 published by Soraisam et al. (2018) and 14 shorter periods in the LMC, published by Yang & Jiang (2011) (see further discussion in Section 4.3). We also plot fitted lines from Soraisam et al. (2018) and Yang & Jiang (2011). The agreement between the lines and our results is evident. Soraisam et al. (2018) found that RSG P–L relation is consistent between the LMC, SMC, Galactic RSGs and the M33 (Yang & Jiang 2011, Yang & Jiang 2012, Kiss et al. 2006 and Soraisam et al. 2018), despite the range of metallicities (Ren et al. 2019).

Figure 4. Sample DASCH (10-d bins) lightcurves with associated power density spectra of three RSGs in the LMC, 003, 043 and 083. Arrows indicate measured pulsational periods (All lightcurves are available in the supplementary material).

Table 2. Coordinates, *K*-band magnitude, period and amplitude of our sample of RSGs in the LMC. Sources as per Section 3.

Ref.	α_{J2000}	δ_{J2000}	P1 (days)	amp1 (mag)	P2 (days)	amp2 (mag)	P3 (days)	amp3 (mag)	K (mag)	σ_K (mag)	M_K (mag)
001	72.3436	−69.4096	610	0.20	1950	0.16	−−	—	7.76	0.04	−10.74
003	72.7445	−69.2341	2290	0.19	−−	—	−−	—	8.36	0.02	−10.14
004	72.8792	−69.2478	490	0.12	674	0.10	2681	0.15	8.24	0.02	−10.26
005	72.9470	−69.3235	365	0.15	−−	—	−−	—	8.74	0.02	−9.76
006	73.3116	−69.2050	−−	—	−−	—	−−	—	7.75	0.02	−10.75
007	73.3269	−69.2842	5000	0.06	−−	—	−−	—	8.36	0.02	−10.14
008	73.3788	−69.2971	−−	—	−−	—	−−	—	8.06	0.02	−10.44
009	73.6536	−69.3395	4340	0.07	−−	—	−−	—	7.61	0.03	−10.89
010	73.6606	−69.1881	755	0.16	2350	0.17	−−	—	7.20	0.03	−11.30
011	73.6642	−69.0768	3970	0.56	−−	—	−−	—	8.66	0.02	−9.84
012	73.7070	−69.5007	1560	0.08	−−	—	−−	—	8.43	0.02	−10.07
014	73.8169	−69.3200	435	0.08	1500	0.07	−−	—	7.37	0.03	−11.13
016	73.8750	−69.4863	565	0.18	−−	—	−−	—	7.66	0.02	−10.84
017	73.8836	−66.8439	715	0.17	3070	0.16	−−	—	7.66	0.02	−10.84
019	73.9243	−69.4401	610	0.27	−−	—	−−	—	7.70	0.02	−10.80
020	73.9511	−69.4018	335	0.08	−−	—	−−	—	7.97	0.02	−10.53
021	74.0986	−69.7031	320	0.06	2510	0.07	−−	—	8.45	0.02	−10.05
023	74.3814	−70.1498	610	0.23	−−	—	−−	—	7.97	0.03	−10.53
024	74.4305	−70.1473	950	0.27	−−	—	−−	—	7.32	0.03	−11.18
025	74.4358	−69.5095	−−	—	−−	—	−−	—	8.56	0.02	−9.94
026	75.5397	−70.4172	−−	—	−−	—	−−	—	8.32	0.02	−10.18
027	75.8137	−70.2949	2375	0.06	−−	—	−−	—	8.72	0.02	−9.78
028	76.0210	−70.3796	4100	0.13	−−	—	−−	—	8.11	0.03	−10.39
029	76.0409	−70.2049	3413	0.06	322	0.05	−−	—	8.39	0.03	−10.11
030	76.0588	−67.2707	990	0.25	−−	—	−−	—	6.78	0.02	−11.72
031	76.1741	−70.7104	2950	0.17	−−	—	−−	—	8.03	0.03	−10.47
032	76.2259	−70.5552	556	0.15	−−	—	−−	—	8.40	0.02	−10.10
033	76.2916	−70.6677	405	0.13	−−	—	−−	—	8.38	0.02	−10.12
034	76.3897	−70.5630	695	0.24	−−	—	−−	—	7.64	0.03	−10.86
035	76.4863	−70.5900	2760	0.19	−−	—	−−	—	8.11	0.03	−10.39
037	76.4981	−70.8032	3675	0.27	−−	—	−−	—	8.32	0.02	−10.18
038	76.6517	−70.5441	2667	0.14	−−	—	−−	—	8.75	0.02	−9.75
039	76.7737	−70.5456	640	0.12	−−	—	−−	—	7.04	0.03	−11.46
040	76.8857	−70.6512	520	0.10	−−	—	−−	—	8.02	0.02	−10.48
042	77.4317	−65.3665	615	0.17	−−	—	−−	—	7.69	0.03	−10.81
043	78.1932	−67.3272	765	0.49	−−	—	−−	—	7.59	0.03	−10.91
044	78.7072	−67.4555	805	0.44	−−	—	−−	—	7.42	0.02	−11.08
045	79.2874	−69.5392	575	0.18	265	0.15	−−	—	7.82	0.02	−10.68
046	79.4848	−69.6737	835	0.07	−−	—	−−	—	8.57	0.02	−9.93
047	79.7636	−69.6653	3650	0.33	−−	—	375	0.53	7.60	0.03	−10.90
048	79.9720	−69.4593	1750	0.15	−−	—	−−	—	8.22	0.03	−10.28
049	80.0984	−69.5575	520	0.18	−−	—	−−	—	7.98	0.02	−10.52
050	80.3665	−69.5045	1635	0.13	−−	—	−−	—	8.14	0.02	−10.36
051	80.6295	−69.5681	−−	—	−−	—	−−	—	8.65	0.02	−9.85
052	80.7615	−69.3436	285	0.06	−−	—	−−	—	8.51	0.02	−9.99
053	80.8916	−69.3186	1250	0.08	−−	—	380	0.09	8.90	0.02	−9.60
054	80.9317	−65.6999	675	0.28	−−	—	−−	—	7.74	0.05	−10.76
056	81.0804	−69.6470	4900	0.12	−−	—	−−	—	6.81	0.02	−11.69
057	81.4369	−69.0802	510	0.13	2470	0.13	−−	—	7.99	0.02	−10.51
060	81.5671	−66.1164	510	0.27	−−	—	−−	—	8.03	0.03	−10.47
061	81.6141	−69.1822	655	0.37	3510	0.23	−−	—	7.70	0.02	−10.80
062	81.6176	−69.1327	405	0.11	2650	0.10	−−	—	8.48	0.02	−10.02
063	81.6450	−68.8611	3210	0.19	−−	—	−−	—	7.26	0.03	−11.24
065	81.6780	−68.9536	435	0.14	2250	0.12	−−	—	8.55	0.02	−9.95
067	81.7929	−69.2715	3700	0.26	−−	—	−−	—	8.78	0.02	−9.72
070	81.8669	−69.0100	3670	0.57	−−	—	−−	—	8.32	0.02	−10.18
071	81.8737	−67.2370	1230	0.15	−−	—	−−	—	7.97	0.03	−10.53
072	81.8931	−66.8917	650	0.23	−−	—	−−	—	7.84	0.03	−10.66
074	81.9479	−69.2224	3735	0.50	−−	—	−−	—	7.60	0.03	−10.90
075	81.9630	−67.3011	−−	—	−−	—	−−	—	8.60	0.02	−9.90
076	81.9631	−69.1794	1250	0.09	−−	—	−−	—	8.29	0.03	−10.21
077	82.0249	−69.1204	1270	0.13	−−	—	−−	—	8.15	0.03	−10.35

Table 2 – *continued*

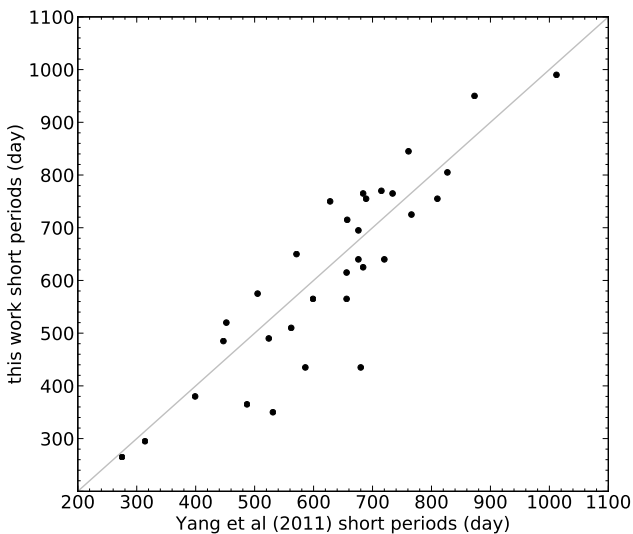| Ref.	α_{J2000}	δ_{J2000}	P1 (days)	amp1 (mag)	P2 (days)	amp2 (mag)	P3 (days)	amp3 (mag)	K (mag)	σ_K (mag)	M_K (mag)
079	82.0642	−66.9813	510	0.18	4100	0.16	––	—	8.09	0.02	−10.41
080	82.0662	−69.2003	––	—	––	—	––	—	8.51	0.02	−9.99
081	82.0775	−69.1264	1665	0.34	––	—	––	—	8.31	0.03	−10.19
082	82.1163	−69.2159	3735	0.20	––	—	370	0.21	8.38	0.03	−10.12
083	82.1202	−68.1189	770	0.21	––	—	––	—	7.48	0.02	−11.02
084	82.1264	−69.0123	––	—	––	—	––	—	8.50	0.02	−10.00
085	82.1314	−69.0920	480	0.16	––	—	––	—	8.05	0.03	−10.45
087	82.1799	−67.3079	2570	0.10	––	—	––	—	8.58	0.02	−9.92
091	82.2532	−68.7760	––	—	––	—	––	—	8.44	0.02	−10.06
092	82.2645	−69.1128	640	0.26	––	—	––	—	7.90	0.02	−10.60
093	82.2729	−67.3049	2275	0.04	––	—	––	—	8.57	0.02	−9.93
094	82.2850	−69.2051	3390	0.24	––	—	370	0.27	8.35	0.04	−10.15
097	82.3650	−69.1473	765	0.31	––	—	––	—	7.30	0.02	−11.20
098	82.3934	−66.9245	500	0.40	––	—	––	—	8.73	0.02	−9.77
099	82.4258	−68.9548	845	0.15	––	—	––	—	6.89	0.03	−11.61
100	82.4332	−69.0972	520	0.18	3775	0.16	––	—	7.88	0.02	−10.62
101	82.4782	−69.0710	295	0.06	––	—	––	—	8.41	0.02	−10.09
102	82.4789	−67.3102	750	0.09	––	—	365	0.10	7.79	0.02	−10.71
103	82.5095	−67.0459	575	0.12	––	—	––	—	7.97	0.02	−10.53
104	82.5191	−68.7913	3445	0.06	––	—	––	—	8.77	0.02	−9.73
105	82.5206	−69.0666	810	0.12	1900	0.11	––	—	8.81	0.02	−9.69
106	82.5399	−69.1844	3935	0.09	––	—	––	—	8.64	0.02	−9.86
107	82.5873	−67.3348	625	0.14	2665	0.16	––	—	7.45	0.03	−11.05
108	82.5921	−67.1088	3570	0.29	––	—	––	—	8.60	0.02	−9.90
109	82.6095	−69.5068	2235	0.23	––	—	––	—	8.48	0.02	−10.02
111	82.6481	−68.9898	365	0.19	4330	0.25	670	—	7.55	0.02	−10.95
112	82.6482	−67.2012	1160	0.07	––	—	––	—	8.85	0.02	−9.65
113	82.6727	−69.2594	4265	0.33	––	—	––	—	7.59	0.02	−10.91
114	82.6749	−69.0898	2155	0.13	––	—	––	—	8.76	0.02	−9.74
115	82.6882	−67.1332	190	0.10	2770	0.12	––	—	8.43	0.02	−10.07
116	82.7179	−67.2929	200	0.10	2610	0.11	––	—	8.83	0.02	−9.67
118	82.7550	−69.1831	365	0.22	––	—	––	—	8.33	0.03	−10.17
119	82.7643	−69.0945	––	—	––	—	––	—	8.58	0.03	−9.92
120	82.7674	−69.3175	652	0.26	––	—	––	—	7.63	0.03	−10.87
121	82.7886	−67.4319	565	0.19	3175	0.19	––	—	7.63	0.02	−10.87
122	82.8144	−69.0664	3255	0.09	––	—	––	—	8.22	0.02	−10.28
123	82.8269	−69.1578	––	—	––	—	––	—	8.63	0.02	−9.87
124	82.9034	−66.5021	725	0.30	––	—	––	—	7.37	0.02	−11.13
125	82.9475	−67.3842	––	—	––	—	––	—	8.59	0.02	−9.91
126	83.0367	−67.1885	––	—	––	—	––	—	8.69	0.03	−9.81
128	83.1143	−69.2813	465	0.14	––	—	––	—	7.96	0.02	−10.54
129	83.1306	−69.3404	965	0.06	––	—	365	0.07	8.63	0.02	−9.87
130	83.1471	−69.1310	––	—	––	—	––	—	8.26	0.02	−10.24
131	83.2093	−67.4625	440	0.12	––	—	––	—	8.05	0.03	−10.45
132	83.2817	−66.8016	485	0.22	2350	0.22	––	—	8.61	0.02	−9.89
134	83.3617	−67.0704	350	0.07	1669	0.07	––	—	7.82	0.03	−10.68
135	83.3733	−67.5271	––	—	––	—	––	—	8.82	0.02	−9.68
136	83.4356	−67.4047	380	0.08	2350	0.08	––	—	8.49	0.02	−10.01
137	83.4674	−69.1871	645	0.20	––	—	––	—	7.90	0.02	−10.60
138	83.5586	−68.9789	––	—	––	—	––	—	7.96	0.02	−10.54
139	83.5812	−68.9935	––	—	––	—	––	—	8.53	0.02	−9.97
140	83.5893	−69.3667	295	0.10	1550	0.09	––	—	8.89	0.02	−9.61
141	83.6407	−69.2507	2665	0.18	––	—	––	—	8.28	0.02	−10.22
142	83.6959	−69.4835	––	—	––	—	––	—	9.02	0.03	−9.48
143	83.8088	−67.7322	710	0.35	––	—	––	—	8.02	0.02	−10.48
144	83.8288	−67.0388	415	0.19	575	0.16	2550	0.16	8.34	0.03	−10.16
145	83.8522	−69.0676	310	0.12	850	0.15	1950	0.14	8.23	0.03	−10.27
146	83.8680	−66.9340	755	0.28	––	—	––	—	7.26	0.03	−11.24
147	83.8867	−69.0720	––	—	––	—	––	—	8.20	0.02	−10.30
148	83.9326	−68.8558	2620	0.13	––	—	––	—	8.04	0.02	−10.46
149	83.9665	−69.3748	1700	0.08	––	—	––	—	8.45	0.02	−10.05
151	84.0266	−68.9447	––	—	––	—	––	—	8.44	0.02	−10.06

Table 2 – *continued* .

Ref.	α_{J2000}	δ_{J2000}	P1 (days)	amp1 (mag)	P2 (days)	amp2 (mag)	P3 (days)	amp3 (mag)	K (mag)	σ_K (mag)	M_K (mag)
154	84.1061	−66.9273	750	0.23	--	—	--	—	7.50	0.03	−11.00
155	84.1115	−69.3976	465	0.19	--	—	--	—	7.81	0.02	−10.69
156	84.1691	−69.3879	--	—	--	—	--	—	8.81	0.02	−9.69
158	84.3599	−68.7945	1800	0.10	--	—	--	—	8.23	0.02	−10.27
159	84.3777	−69.0425	3560	0.10	--	—	--	—	8.72	0.02	−9.78
160	84.4037	−69.4899	--	—	--	—	--	—	8.21	0.02	−10.29
162	84.4379	−69.3468	--	—	--	—	--	—	7.72	0.03	−10.78
163	84.4945	−69.2400	--	—	--	—	--	—	8.38	0.02	−10.12
166	84.5755	−69.2951	1965	0.13	--	—	--	—	8.30	0.02	−10.20
167	84.6418	−69.3422	4560	0.13	--	—	--	—	8.51	0.02	−9.99
168	84.9426	−69.3245	--	—	--	—	--	—	8.47	0.02	−10.03
170	85.0320	−69.3347	2200	0.14	--	—	--	—	8.29	0.03	−10.21
172	85.1022	−69.3548	--	—	--	—	--	—	7.85	0.03	−10.65
173	85.1058	−69.2584	3215	0.20	--	—	--	—	8.78	0.02	−9.72
174	85.1541	−69.4390	--	—	--	—	--	—	8.32	0.02	−10.18
175	85.1826	−69.3662	1300	0.16	--	—	--	—	7.44	0.02	−11.06
177	85.2308	−69.3904	2570	0.13	--	—	--	—	7.54	0.02	−10.96
178	85.2470	−69.3101	715	0.12	2515	0.13	--	—	7.49	0.03	−11.01
179	85.2712	−69.0784	3445	0.15	--	—	--	—	7.98	0.02	−10.52
180	85.2789	−69.2874	2315	0.16	--	—	--	—	7.77	0.02	−10.73
181	85.2948	−69.6345	--	—	--	—	--	—	7.63	0.02	−10.87
182	85.3408	−69.5303	435	0.16	2455	0.24	--	—	7.82	0.03	−10.68
183	85.3731	−69.4544	2100	0.07	--	—	--	—	8.45	0.02	−10.05
184	85.4309	−69.4710	2778	0.07	--	—	--	—	8.41	0.02	−10.09
185	85.4335	−69.2008	3215	0.21	--	—	--	—	8.40	0.02	−10.10
186	85.4590	−69.3543	265	0.07	1530	0.06	--	—	8.56	0.02	−9.94
187	85.5031	−69.1936	4100	0.09	1055	0.10	--	—	8.68	0.02	−9.82
188	85.6608	−69.1643	2245	0.14	--	—	--	—	8.82	0.02	−9.68
189	85.7585	−69.0972	445	0.05	--	—	--	—	8.37	0.03	−10.13
195	81.9115	−69.4793	2550	0.13	--	—	--	—	8.22	0.02	−10.28
199	83.0805	−67.5223	3355	0.16	--	—	--	—	8.05	0.03	−10.45
200	83.8292	−67.0387	415	0.19	--	—	--	—	8.34	0.03	−10.16
205	83.2494	−68.5986	--	—	--	—	--	—	7.65	0.03	−10.85
208	80.4833	−67.2127	2665	0.07	--	—	--	—	8.20	0.03	−10.30
209	78.5745	−67.3423	1365	0.05	--	—	--	—	8.27	0.02	−10.23
210	79.9719	−68.0677	750	0.09	1625	0.11	--	—	7.20	0.02	−11.30
216	86.1350	−70.6063	580	0.12	2565	0.13	--	—	7.93	0.03	−10.57
217	83.0539	−66.9883	430	0.14	2570	0.18	--	—	8.42	0.02	−10.08
219	82.5861	−66.8839	3650	0.17	--	—	--	—	7.72	0.03	−10.78
220	83.1484	−67.9192	770	0.28	--	—	--	—	7.64	0.02	−10.86
223	85.6478	−69.1467	2100	0.13	--	—	--	—	7.71	0.02	−10.79
225	74.4305	−70.1473	955	0.27	--	—	--	—	7.32	0.03	−11.18
227	82.0619	−66.5461	445	0.27	--	—	--	—	8.84	0.02	−9.66

Figure 7a shows period distribution relative to the Soraisam et al. (2018) fit line for our Galactic RSGs, with different fractional parallax uncertainty limits (15% and 25%). We remind the reader that the uncertainties of the DR2 parallaxes need to be treated with caution (see Section 2.2 for further discussion). The RSGs form two distinct groups: (i) a presumed fundamental or low overtone sequence, and (ii) long secondary periods with more scatter. The LSP scatter is discussed further in Section 4.4. We associate the shorter periods with the fundamental or low overtone modes of pulsation (Stothers & Leung 1971, Li & Gong 1994, Guo & Li 2002, Kiss et al. 2006) that are stochastically driven by convective motions in the envelope (Schwarzschild 1975, Christensen-Dalsgaard et al. 2001, Bedding 2003, Kiss et al. 2006).

The luminosity boundaries for identifying RSGs vary in the literature between $M_{bol}= −5$ mag (Maeder & Meynet 2000) and $M_{bol}= −7.0$ mag (Massey & Olsen 2003, Wood et al. 1983) for the lower limits, to $M_{bol} = −9$ mag (Maeder & Meynet 2000) and $M_{bol} = −10.0$ mag for the upper limits (Humphreys 1986). The upper limit corresponds to the Eddington luminosity, which indicates a stability boundary that prevents massive stars from evolving to cooler temperatures (Humphreys 1986, de Jager et al. 1991, Nota & Lamers 1997). It is a point where the radiation pressure can overcome gravity in the atmosphere of a star, making it unstable. This causes a significant mass loss in massive stars that are evolving to the right of the Hertzsprung–Russell diagram when cooling (Lamers & Levesque 2017, Levesque 2017).

Assuming that $m_{bol} \approx m_K + 3$ (as per Josselin et al. 2000), we set boundaries of our P–L diagrams between $M_K \approx −7.0$ mag for the faintest and −12.0 mag for the brightest objects. W Cep and μ Cep, ($M_K < −12.65$ mag and $M_K = −13.0$ mag, respectively) along with SS And,

Figure 5. Comparison of shorter periods of 32 RSGs in the LMC, from this study with periods published by Yang et al. (2011) . The grey line shows equality.

W Tri and IS Gem ($M_K = -6.72$ mag, $M_K = -6.33$ mag and $M_K = -2.87$ mag, respectively) fall outside our P–L diagrams.

Note that the histograms in Fig. 7a include Galactic RSGs that are brighter than $M_K = -9.0$ mag. This corresponds to $M_{bol} = -6$ mag. We adopted this cutoff for the presentation of the plot because it is the average of the two published lower limits of $M_{bol} = -5$ mag (Maeder & Meynet 2000) and $M_{bol} = -7.0$ mag (Massey & Olsen 2003, Wood et al. 1983).

4.2 Galactic RSGs

Figure 8 presents period–M_K relations for RSGs in our galactic sample. For convenience, the stars are labelled with their General Catalogue of Variable Stars (GCVS) names and error bars showing calculated M_K uncertainties. Parallax uncertainty was the only factor included in the calculated M_K uncertainties as majority of the K-band magnitude uncertainties were unavailable.

We found 10 stars with relatively large M_K uncertainties (> 1.0 mag; Y Lyn, RV Hya, SU Per, VX Sgr, SS And, BU Gem, NO Aur, μ Cep, W Ind, W Cep) and it would be interesting to see their P–L relations with improved parallax measurements, anticipated in Gaia DR3.

Global astrometric satellites like Hipparcos and Gaia are able to measure absolute parallaxes, that is, without zero-point error, but this capability is susceptible to various instrumental effects which can lead to a small offset in the parallaxes (Lindegren et al. 2018). We investigated an impact of the zero-point offset of −0.1 mas (Khan et al. 2019) on the P–L relation of the Galactic RSGs. In Fig. 8 we show that the adjusted parallaxes can significantly affect the absolute magnitudes of the most distant stars, with SU Per, RW Cyg, ST Cep, CL Car, RT Car and T Per shifted towards fainter values by ∼ 0.5 mag.

Overall, the indicated periods of ASAS and AAVSO data agreed well for majority of the sample. We favored higher

quality lightcurves where they indicated different pulsational frequencies (seven stars). Among those, we found three objects with more reliable data from AAVSO (T Per, AO Cru, WY Gem) and four from ASAS (TZ Cas, EV Car, XY Lyr, SS And). Similarly to Yang & Jiang (2011)(figure 10), our determined periods show positive correlation with the amplitudes (Fig. 9), which is expected for solar–like variations (Kjeldsen & Bedding 1995).

As concluded by Kiss et al. (2006), the periods of RSGs can be divided into two groups, pulsations with periods of 300–1000 d and LSPs with periods of a few thousand days. In total, we found 40 shorter periods in 25 stars and 23 LSPs in 23 stars. Some lightcurves were noisy and their periodicities could not be determined.
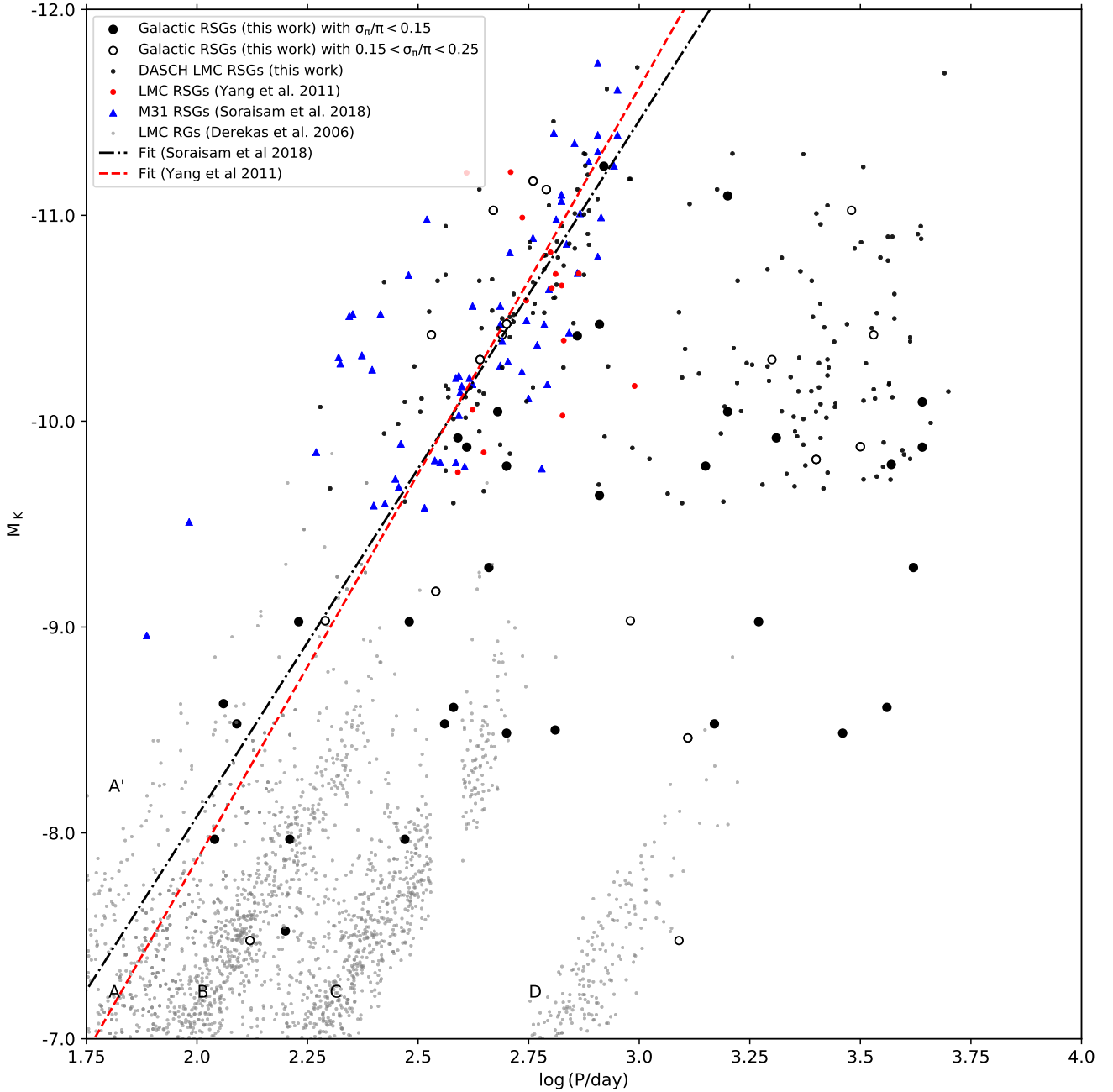
4.3 RSGs in the LMC

Similarly to our Galactic sample, RSGs in the LMC show complex light variations on time scales that range from months to several years. We were able to observe two types of variation – pulsations similar to oscillations in other types of stars and a long secondary period, unique to red giants and supergiants.

The P–L relation we have found agrees well with previous works. The fraction of stars for which we could detect periods (83%) is significantly greater than the 51% found by Yang & Jiang (2011). We explain this difference by the fact that the DASCH observations cover three to six times longer in time. We also found LSPs in 94 stars (or 55%).

In Figure 7b we show a good agreement between distributions of the DASCH periods (92 shorter and 95 long secondary periods) and the 47 shorter periods published in Yang & Jiang (2011)). We note that we do not show LSPs, published by Yang & Jiang 2011 because they were based on only 3000 d of data (mostly ASAS), which we consider too short for a reliable detection of LSPs. Thus, our P–L diagram in Fig. 6 shows only shorter periods, published in Yang & Jiang (2011) and only those for which we could not identify periods from the DASCH data (14 objects in total). They lay along the Soraisam et al. (2018) best fit line, in a good agreement with the detected shorted periods in this study.

4.4 Comparing red supergiants to red giants

In Figure 8 we show the corresponding LMC sequences from the Massive Compact Halo Object (MACHO) survey data, analysed by Derekas et al. (2006), for a comparison. The sequences are labelled C (fundamental), A′, A, B (overtones) and D (LSPs) following the naming conventions by Wood et al. (1999). The sequence A′ comprise the shortest periods and smallest amplitudes (Soszyński et al. 2004). LSPs are common for RSGs and RGs but the origin of this phenomenon has been a long-standing unknown (Stothers 2010). The RSGs are clearly not in line with the relatively tight sequences of the red giants, as might have been expected. The RSGs are clustered in two groups: pulsations (presumably fundamental and low overtones) and LSPs (around extended sequence D of the RGs), with the LSPs group being much more dispersed. In general, the observed scatter in RSGs may be a result of the fact that the evolutionary tracks of different masses overlap in luminosity,

Figure 6. Period–luminosity relation of our Galactic and LMC samples. Galactic RSGs with different fractional parallax uncertainty limits are shown as black filled (15%) and empty circles (25%). Best fit lines for the LMC and M31 are from Yang & Jiang (2011) and Soraisam et al. (2018), respectively.
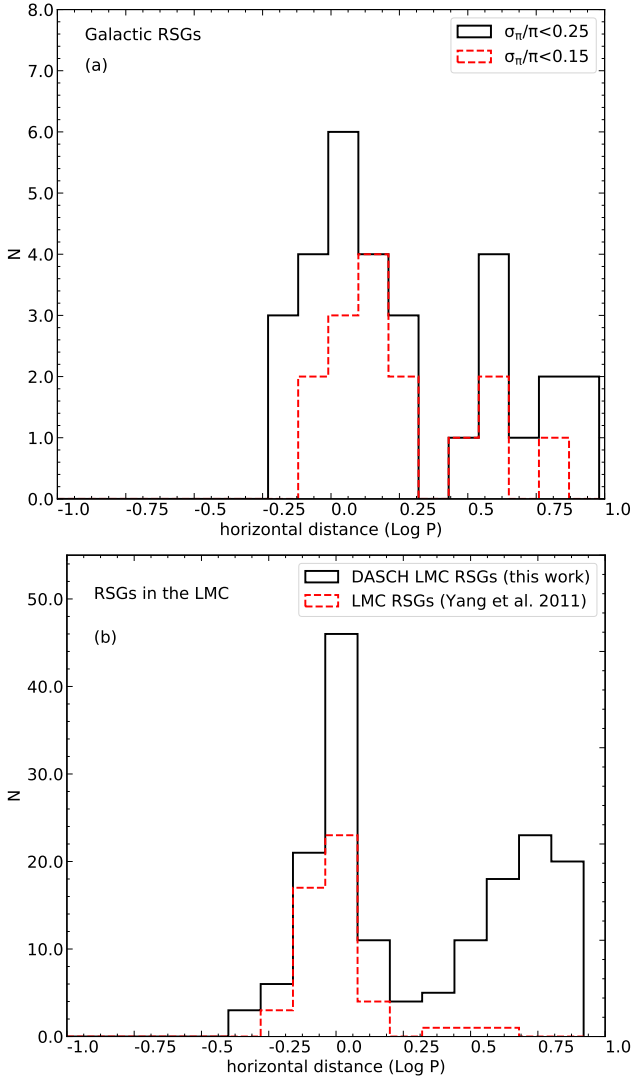
which in turn can affect their periods (Soraisam et al. 2018). Models show that the overlap can be even stronger, depending on how other underlying processes such as convection, binarity and mass loss (which are currently not entirely understood) are treated (Levesque 2017). These add uncertainty to any potential extragalactic distance estimates based on the P–L relations of RSGs.

An interesting feature of the presented P–L relations is a lack of stars between RSGs and RGs (between $M_K \approx -8.5$ and $M_K \approx -9.5$ mag). Future study of objects that occupy

this gap should reveal what transition in the P–L diagram they form between RSG and RGs.

4.5 RSGs in M31

Soraisam et al. (2018) studied RSGs in M31 (Andromeda) and found that the P–L relation of the RSGs agree well across the nearest galaxies (SMC, LMC, Milky Way, M31). They compared the analyzed P–L relation with the theoretical one based on MESA models and found their two groups

Figure 7. (a) Period distribution from the Soraisam et al. (2018) fit line for our Galactic and LMC samples, as presented on Fig. 6. (b) (RSGs in the LMC) Distribution of the detected DASCH periods is compared with shorter periods published in Yang & Jiang (2011). The two groups: (i) a presumed fundamental or low overtone sequence, and (ii) long secondary periods are distinct.

of shorter periods to pulsate in the fundamental radial and low overtone modes.

The majority of the shorter period M31 RSGs (shown as blue triangles in Fig. 6) overlap with our Galactic and the LMC shorter periods, around the extended sequence A of the RGs. In general, the agreement is good, with a few stars in M31 that seem to pulsate with shorter periods than expected for their luminosities. Soraisam et al. (2018) suggested that these stars may have different masses but overlapping luminosities. No LSPs have been published in the Andromeda galaxy study as it is based on the five-year survey, which is too short for an accurate detection of LSPs.

5 CONCLUSIONS

Using long-term lightcurves from several campaigns we analysed over 220 RSGs in the LMC and the Milky Way and studied their main pulsational characteristics. Parallaxes from Gaia Data Release 2 allowed us to tighten the P–L relations of our Galactic sample, where we found 40 shorter and 23 longer periods. Our LMC sample contains 142 stars, with most having a usable observation time of approximately 50 years. Among those, we found 92 shorter and 95 longer periods.

We found that the P-M_K relations agree well with the literature (Yang & Jiang 2011, Soraisam et al. 2018). When compared to the red giants, it is clear that the RSGs do not follow the same sequences. Periods of RSGs form two groups: (i) a pronounced group on the P–L diagram (Fig. 6) with periods of 300–1000 d, and (ii) the LSP group, with periods between 1000 and 8000 d, that is much more dispersed. We considered an impact of the Gaia zero-point shift in parallaxes on the P–L relations of distant RSGs to be significant.
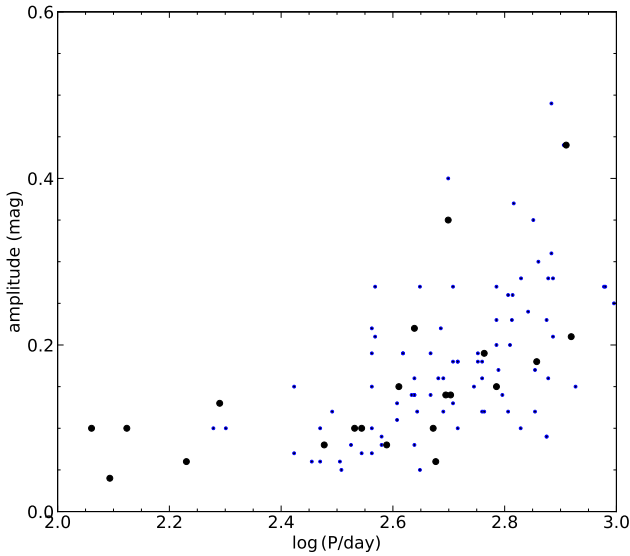
It is clear that pulsations following a P–L relation are present in most RSGs in the Local Group and that this relation does not depend on the metallicity (Ren et al. 2019). In order to consider RSGs "standard candles" (as suggested by Glass 1979), factors like the abundance of irregular variables, mass loss, dust production and the additional sources of long-period variability need to be further explored. Each of these mechanisms can contribute to changes in the apparent magnitude of RSGs, causing periodic or stochastic fluctuations in their lightcurves, and result in a further dispersion of their P–L relations.

Without a theoretical basis, further investigation of origins of the LSPs and variability of RSGs in general, is difficult. Long-term photometric monitoring is one of the main challenges in studying pulsations of RGSs, and there may be many years before we expect better lightcurves. More precise distance measurements from future Gaia data releases may present opportunities for future work.

Figure 8. Period–absolute *K* magnitude relations for our Galactic RSG sample, with fractional parallax uncertainty limit < 0.5. M_K uncertainties are shown as vertical lines. Red circles indicate shifted absolute magnitudes of the RSGs (RSGs with the DR2 parallaxes only), where a Gaia zero-point error of 0.1 mas has been adopted. See Section 2.2 for further discussion. W Cep, μ Cep with their respective calculated absolute magnitudes of $M_K < -12.65$ mag and $M_K = -12.97$ mag are not shown, neither are SS And, W Tri, IS Gem (calculated absolute *K* magnitudes −6.72, −6.33, −2.87 mag, respectively).

REFERENCES

Asaki Y., Deguchi S., Imai H., Hachisuka K., Miyoshi M., Honma M., 2010, ApJ, 721, 267
Bailer-Jones C. A. L., 2015, PASP, 127, 994
Bailer-Jones C. A. L., Rybizki J., Fouesneau M., Mantelet G., Andrae R., 2018, AJ, 156, 58
Bedding T. R., 2003, Ap&SS, 284, 61
Boyer M. L., et al., 2011, AJ, 142, 103
Cardelli J. A., Clayton G. C., Mathis J. S., 1989, ApJ, 345, 245
Catchpole R. M., Feast M. W., 1981, MNRAS, 197, 385
Chiavassa A., Freytag B., Schultheis M., 2018, A&A, 617, L1
Christensen-Dalsgaard J., Kjeldsen H., Mattei J. A., 2001, ApJ, 562, L141

Cutri R. M., et al., 2003, VizieR Online Data Catalog, 2246
Derekas A., Kiss L. L., Bedding T. R., Kjeldsen H., Lah P., Szabó G. M., 2006, ApJ, 650, L55
Ducati J. R., 2002, VizieR Online Data Catalog, 2237
Feast M. W., Catchpole R. M., Carter B. S., Roberts G., 1980, MNRAS, 193, 377
Gaia Collaboration 2016, VizieR Online Data Catalog, 1337
Gaia Collaboration 2018, VizieR Online Data Catalog, 1345
Gaia Collaboration et al., 2016, A&A, 595, A1
Gaia Collaboration et al., 2018, A&A, 616, A1
Gezari D. Y., Pitts P. S., Schmitz M., 1999, VizieR Online Data Catalog, 2225
Glass I. S., 1979, MNRAS, 186, 317
Grindlay J., Tang S., Los E., Servillat M., 2012, in Griffin E., Hanisch R., Seaman R., eds, IAU Symposium Vol. 285, New Horizons in Time Domain Astronomy. pp 29–34 (arXiv:1211.1051), doi:10.1017/S1743921312000166
Guo J. H., Li Y., 2002, ApJ, 565, 559
Humphreys R. M., 1986, in De Loore C. W. H., Willis A. J., Laskarides P., eds, IAU Symposium Vol. 116, Luminous Stars

Figure 9. The period–amplitude relationship of RSGs that are thought to be pulsating in the fundamental or low overtone modes. The LMC sample is shown as small blue circles, and Galactic RSGs are presented as large black circles. Note that our amplitudes are half of the peak-to peak amplitudes. The plot shows Galactic RSGs with $\sigma_\pi/\pi = 0.25$.

and Associations in Galaxies. pp 45–57

Humphreys R. M., Davidson K., 1979, ApJ, 232, 409

Jayasinghe T., et al., 2018, MNRAS, 477, 3145

Josselin E., Blommaert J. A. D. L., Groenewegen M. A. T., Omont A., Li F. L., 2000, A&A, 357, 225

Jurcevic J. S., Pierce M. J., Jacoby G. H., 2000, MNRAS, 313, 868

Kastner J. H., Thorndike S. L., Romanczyk P. A., Buchanan C. L., Hrivnak B. J., Sahai R., Egan M., 2008, AJ, 136, 1221

Khan S., et al., 2019, arXiv e-prints,

Kiss L. L., Szabó G. M., Bedding T. R., 2006, MNRAS, 372, 1721

Kjeldsen H., Bedding T. R., 1995, A&A, 293, 87

Kusuno K., Asaki Y., Imai H., Oyama T., 2013, ApJ, 774, 107

Lamers H. J. G. L. M., Levesque E. M., 2017, Understanding Stellar Evolution, doi:10.1088/978-0-7503-1278-3.

Leavitt H. S., Pickering E. C., 1912, Harvard College Observatory Circular, 173, 1

Lenz P., Breger M., 2005, Communications in Asteroseismology, 146, 53

Levesque E. M., 2017, Astrophysics of Red Supergiants, doi:10.1088/978-0-7503-1329-2.

Levesque E. M., Massey P., Olsen K. A. G., Plez B., Meynet G., Maeder A., 2006, ApJ, 645, 1102

Li Y., Gong Z. G., 1994, A&A, 289, 449

Lindegren L., et al., 2018, A&A, 616, A2

Lomb N. R., 1976, Ap&SS, 39, 447

Luri X., et al., 2018, A&A, 616, A9

Lutz T. E., Kelker D. H., 1973, PASP, 85, 573

Maeder A., Meynet G., 2000, ARA&A, 38, 143

Massey P., Olsen K. A. G., 2003, AJ, 126, 2867

Massey P., Plez B., Levesque E. M., Olsen K. A. G., Clayton G. C., Josselin E., 2005, ApJ, 634, 1286

Massey P., Silva D. R., Levesque E. M., Plez B., Olsen K. A. G., Clayton G. C., Meynet G., Maeder A., 2009, ApJ, 703, 420

Meynet G., et al., 2015, A&A, 575, A60

Mould J., 1987, PASP, 99, 1127

Nota A., Lamers H., eds, 1997, Luminous Blue Variables: Massive Stars in Transition Astronomical Society of the Pacific Conference Series Vol. 120

Percy J. R., Khatu V. C., 2014, Journal of the American Association of Variable Star Observers (JAAVSO), 42, 1

Pietrzyński G., et al., 2019, Nature, 567, 200

Pojmański G., 2004, Astronomische Nachrichten, 325, 553

Ren Y., Jiang B.-W., Yang M., Gao J., 2019, ApJS, 241, 35

Riess A. G., et al., 2018, ApJ, 861, 126

Scargle J. D., 1982, ApJ, 263, 835

Schwarzschild M., 1975, ApJ, 195, 137

Soraisam M. D., et al., 2018, ApJ, 859, 73

Soszyński I., Udalski A., 2014, The Astrophysical Journal, 788, 13

Soszyński I., Udalski A., Kubiak M., Szymanski M., Pietrzynski G., Zebrun K., Szewczyk O., Wyrzykowski L., 2004, Acta Astron., 54, 129

Soszyński I., et al., 2007, Acta Astron., 57, 201

Stassun K. G., Torres G., 2018, ApJ, 862, 61

Stothers R. B., 2010, ApJ, 725, 1170

Stothers R., Leung K. C., 1971, A&A, 10, 290

Tabur V., Bedding T. R., Kiss L. L., Moon T. T., Szeidl B., Kjeldsen H., 2009, MNRAS, 400, 1945

Tang S., Grindlay J., Los E., Servillat M., 2013, PASP, 125, 857

Wasatonic R. P., Guinan E. F., Durbin A. J., 2015, PASP, 127, 1010

Wood P. R., 2000, Publ. Astron. Soc. Australia, 17, 18

Wood P. R., Bessell M. S., 1985, PASP, 97, 681

Wood P. R., Bessell M. S., Fox M. W., 1983, ApJ, 272, 99

Wood P. R., et al., 1999, in Le Bertre T., Lebre A., Waelkens C., eds, IAU Symposium Vol. 191, Asymptotic Giant Branch Stars. p. 151

Yang M., Jiang B. W., 2011, ApJ, 727, 53

Yang M., Jiang B. W., 2012, ApJ, 754, 35

Zhang B., Reid M. J., Menten K. M., Zheng X. W., 2012, ApJ, 744, 23

Zinn J. C., Pinsonneault M. H., Huber D., Stello D., 2018, arXiv e-prints,

de Jager C., de Koter A., Carpay J., Nieuwenhuijzen H., 1991, A&A, 244, 131

van Leeuwen F., 2007, A&A, 474, 653

APPENDIX A: LIGHT CURVES AND POWER SPECTRA

Supplementary material is available online.

This paper has been typeset from a TeX/LaTeX file prepared by the author.